

Wave impact pressures on vertical cylinders

D. Zhou, E.S. Chan[†] and W.K. Melville

Ralph M. Parsons Laboratory, Dept. of Civil Engineering, Bldg 48, Massachusetts Institute of Technology, MA 02139, U.S.A.

Laboratory measurements of the pressure distributions on surface-piercing vertical cylinders due to breaking waves are presented. Breaking waves are generated in a repeatable fashion under program control, and both vertical and azimuthal distributions of pressures were measured over many repeats of the experiments. Despite the repeatability of the controllable experimental conditions, it is found that the highest impact pressures are subject to considerable variability, including pressure oscillations, from run to run. This high impact region is found to be localized in space and time, and the variability is attributed to the random dynamics of the breaking wave front and the entrapped air. Thus, despite the repeatability of the upstream incident wave hydrodynamics, it appears that the prediction of the largest pressures is essentially a stochastic problem. For those aspects of flow-structure interaction which do not depend on the higher-frequency impact pressures, these experimental results may be extrapolated to full scale through the use of the pressure impulse.

1. INTRODUCTION

It is often anticipated that wave impact will yield the highest hydrodynamic loads on marine structures. As shown later in this paper, impact pressures can be more than ten times higher than non-impact pressures and the duration of impact is typically a small fraction ($< 1/100$) of the characteristic wave period. Such impulsive loads can lead to unacceptable structural responses, or even structural failure, and a good knowledge of the impact phenomenon is clearly warranted. A detailed study of wave impact on vertical plates has been presented in a series of papers by Chan and Melville¹⁻⁴. This paper presents a study of wave impact on vertical cylinders.

Due to the complex and transient nature of the impact process, studies of wave impact on cylinders have, in the past, been rather limited. Attempts to monitor wave impact forces on cylinders (Honda and Mitsuyasu⁵; Dalton and Nash⁶; Wiegel⁷; Takagi *et al.*⁸) were often limited by the dynamic response of the measurement system when subjected to an impulsive load. This leads to distortions in the force signals which must then be corrected by evaluating the dynamic response of the system. Unfortunately, the dynamics of the measurement system, which involve the force transducer, the model, and the ambient fluid, are typically difficult to evaluate, and the forces are usually taken as measured. Increasing the natural frequency of the force measurement system will reduce the structural vibrations, but this will also imply a reduction in the sensitivity of the force measurement system, leading to a poor signal-to-noise ratio. Despite the limitations of force measurements, the above studies did indicate the

significance of impact forces compared to non-impact forces. For vertical cylinders, the impact force can be five to seven times higher than predictions using Morrison's equations and linear theory (Honda and Mitsuyasu⁵).

Theoretical predictions of wave impact forces on cylinders have also been limited. Empirical models to estimate impact forces on cylinders (Wiegel⁷, Sawaragi and Nochino⁹, and Tanimoto *et al.*¹⁰) have typically taken the form $F = d(mv)/dt$; where F is the impact force, m is the added mass and v is the fluid velocity. Unfortunately, both the added mass and the fluid velocity are quantities dependent on the interaction between the fluid and the structure and at best can only be approximated. The added mass term is usually approximated by the value corresponding to a two dimensional problem – that of an infinitely long cylinder striking the surface of still water; and the fluid velocity is typically approximated by the phase velocity of the wave. However, both approximations are inaccurate since wave impact on a vertical cylinder is three-dimensional and the fluid velocity near the impact zone can be more than twice the phase velocity if the impact is associated with wave breaking (Peregrine¹¹).

Following the success in the numerical modelling of highly nonlinear waves (Longuet-Higgins and Cokelet¹²; Vinje and Brevig¹³), attempts have also been made to simulate wave impact loads on cylinders. However, current numerical models can only simulate a two dimensional problem, such as wave impact on a horizontal cylinder parallel to the wave crest (Vinje and Brevig¹⁴). Attempts to simulate wave impact on a vertical cylinder have been made by Takagi *et al.*⁸. This is based on the assumption that the evolution of the incident wave crest is independent of the presence of the cylinder, and at discrete elevations the force is estimated based on Morrison's equation¹⁵. The above assumption is clearly unsatisfactory, especially if the cylinder

[†]Department of Civil Engineering, National University of Singapore, Kent Ridge, Singapore 0511

Paper accepted July 1990. Discussion closes September 1992

© 1991 Elsevier Science Publishers Ltd

diameter is large compared to the incident wave height. Furthermore, even if the predicted wave kinematics are reasonable, the prediction of wave load is still dependent on the estimates of the inertia and drag coefficients used in the model. These coefficients are unknown values for the highly transient impact process and have been assumed constant by Takagi *et al.*⁸.

A factor which has not been included in previous analyses of wave impact is the dynamics of air during impact. Detailed measurements of wave impact on a vertical wall (Chan and Melville⁴) have shown that air dynamics may play a role at impact; contribution to both the high impact pressures and the pressure oscillations in the impact region. Air dynamics can also lead to significant variability in the impact pressures even when the incident waves are essentially identical. Similar features are obtained for impact on cylinders. This is evident in the results presented by Sawaragi and Nochino⁹. Chan and Melville⁴ further showed that for plunging wave impact, the pressure characteristics also depend significantly on the development of wave breaking just prior to impact. Given the variability in the load maxima at impact, particularly for the same incident wave conditions, it is anticipated that impact pressures are sensitive to small changes in the kinematics of the incident wave front and the geometry of the structural boundary. Neglecting the presence of the structure while simulating the incident wave kinematics, as proposed by Takagi *et al.*⁸, will therefore be erroneous. Unless the dynamics of air is clearly understood, predictions of wave impact forces or pressures will have to be stochastic, relying on statistics obtained from experimental findings. Attempts have been made by Ochi and Tsai¹⁶ to yield statistical predictions of impact pressures on cylinders. The analysis was based on pressures monitored along a vertical profile facing the incident wave front. However, the pressures obtained seem to exhibit little variability, contrary to the results obtained by Chan and Melville³ for cylinders of similar size. A higher variability in the pressure maxima is expected due to the presence of trapped air during impact, and the applicability of Ochi and Tsai's results may be quite limited.

From the above review, it is clear that an improved knowledge of the pressure distributions, pressure characteristics, and the pressure variabilities will lead to a better understanding of the physics of wave impact and a better model for predicting impact forces. This will require a detailed study with a systematic variation of the incident wave conditions and the structure dimensions. Rapid variation of the pressure characteristics in both space and time will further require extremely good control in any experimental studies of the impact phenomenon. Due to the lack of control of the incident wave conditions, it is unlikely that field studies will lead to a fundamental improvement in our understanding of wave impact. However, laboratory studies are possible due to recent advances in experimental control (Chan and Melville⁴). Such a study is presented in this paper.

It is noted that a complete study will necessitate a variation of the incident wave conditions from regular non-breaking waves to waves that plunge on the cylinder. However, this would be very time consuming and in this study we have limited ourselves to the most severe impact condition, namely impact by a plunging

wave. A description of the experiments and the instrumentation is presented in the following section. The characteristics and distributions of the impact pressures, which include the pressure maxima, pressure variability, pressure variation with cylinder locations, and the distributions of mean pressure maxima, are presented in Section 3. Correlation of the results with the wave plunging process is discussed in Section 4. Also discussed are the engineering implications of the results and the extrapolation of results to prototype conditions.

2. THE EXPERIMENTS

The experiments were conducted in a 30 m long wave tank at the Ralph M. Parsons Laboratory, Massachusetts Institute of Technology. The channel is 0.76 m wide and 0.9 m deep and the experiments were conducted with a water depth of 0.6 m. Wave plunging was simulated by generating a frequency modulated wave packet consisting of thirty two discrete frequency components, programmed to yield constructive interference at the desired location. This procedure follows Longuet-Higgins¹⁷ and Greenhow *et al.*¹⁸ and has been tested successfully by Chan¹⁹ and Rapp²⁰. The wave packet is characterised by three dominant parameters – the frequency bandwidth, the wave steepness, and the location of wave breaking. Details of the wave packet are specified in Table 1. By varying the steepness parameter, wave breaking ranging from spilling to plunging may be simulated. The steepness yielding a single plunging wave was used in the experiments. The location of wave breaking in many repeats of the experiment varied by less than 0.003 L along the channel (L is the characteristic wave length), indicating a high degree of repeatability of the experiments.

A typical layout of the experiment is shown in Fig. 1. Pressure measurements were obtained simultaneously using five Kistler 606A quartz transducers. These transducers were mounted rigidly in the cylinder wall along a vertical profile, at elevations ranging from 2.5 cm (0.013 L) to 17.5 cm (0.091 L) above the still water level (Fig. 2). The response time of the 606A

Table 1: Characteristics of the wave packet

Frequency bandwidth $\Delta f/f_c$	= 0.727
Steepness parameter Nak_c	= 0.364
Ideal distance to breaking x_b/k_c	= 27.5

where Δf = frequency bandwidth
= 0.64 Hz

f_c = center frequency (0.88 Hz)

N = number of frequency components (32)

a = component amplitude (0.35 cm)

k_c = center wavenumber (3.25 m^{-1})

x_b = breaking locating

(according to linear superposition)

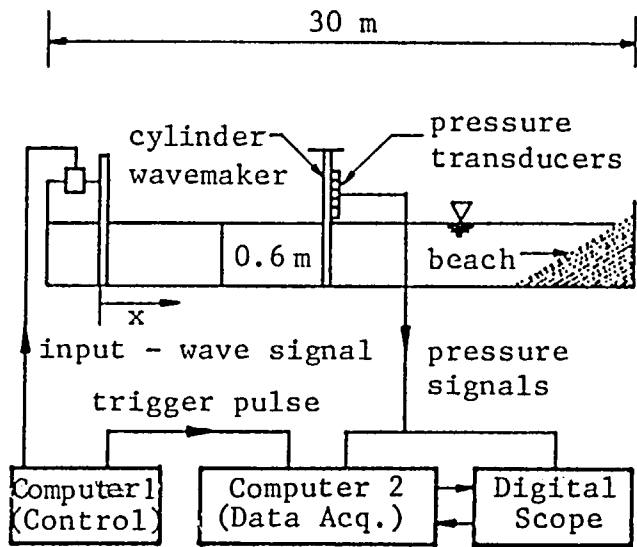


Fig. 1. Layout of experiment

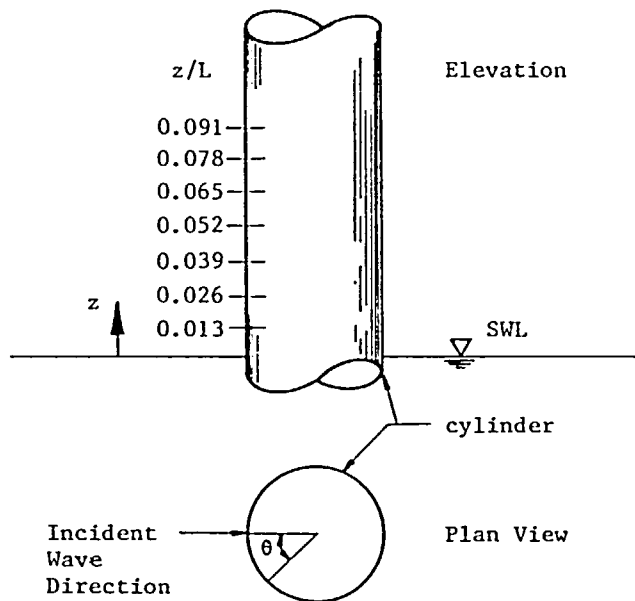


Fig. 2. Transducer locations (z/L) and orientation (θ)

transducer is approximately 1 micro-second, much faster than the rise times of the impulsive pressures (about 1 ms) obtained in the experiments. The pressure range of the transducer is up to 21000 kN/m², far above the highest peak pressure monitored throughout the study (93 kN/m²). Noise levels were less than 0.05 kN/m². In the experiments, the transducers were slightly recessed relative to the cylinder boundary. The recess was filled with silicon grease to transmit the pressure. This arrangement was necessary in order to reduce the strain on the transducer diaphragm caused by temperature differences. The latter was found to yield a slow drift in the pressure signals when the transducer face was flush with the cylinder boundary.

Three cylinders made of PVC, with diameters 12 cm, 17 cm and 22 cm, were used in this series of

experiments. The incident wave parameters were maintained constant throughout the study. For each run of the experiment, the cylinder was first secured rigidly at a predetermined location within the wave breaking zone. The input wave signal (Fig. 1) was then transmitted to the wave generator and just before wave impact on the cylinder a trigger pulse was transmitted to initiate the data acquisition. All pressure signals were recorded digitally with a sampling rate of 20 kHz. The above sampling rate was deemed adequate since the shortest pressure rise time was around 1 ms. On completion of each run of the experiment, the tank was allowed to settle down to its quiescent state before carrying out the next run. This typically took about half an hour, during which time the data was processed.

In this series of studies, the measurements were obtained at cylinder locations $x/L = 3.465, 3.517, 3.568, 3.620, 3.672$ and 3.775 (Fig. 1). At each cylinder location, pressures were also obtained at cylinder orientations $\theta = 0^\circ, 5^\circ, 10^\circ, 20^\circ, 30^\circ, 40^\circ, 50^\circ$ and 60° (Fig. 2). Experiments were repeated at each cylinder location and orientation and details of the results are presented in Zhou²¹. Selected results are presented in this paper.

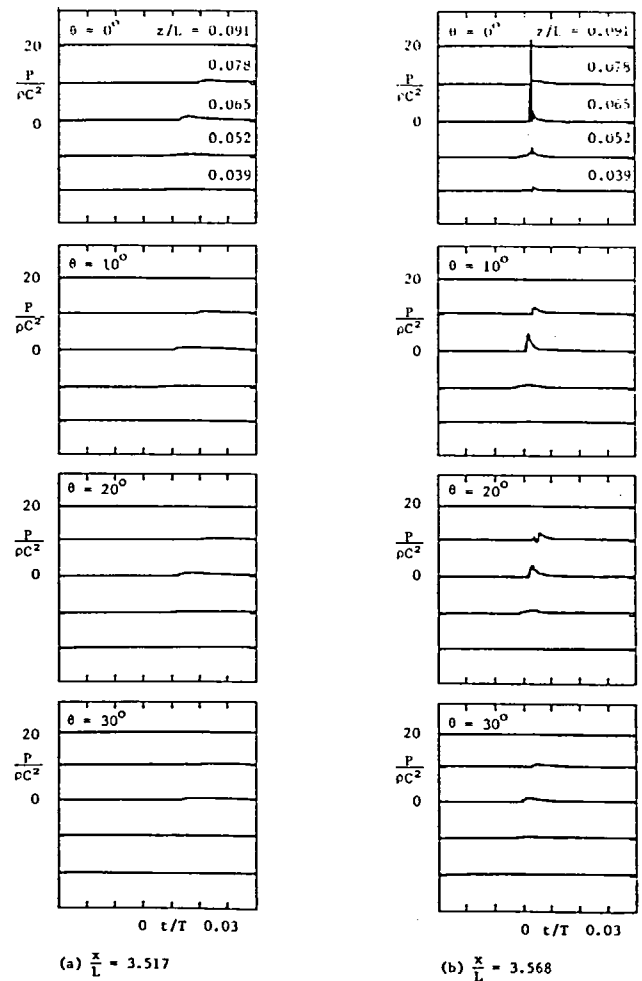
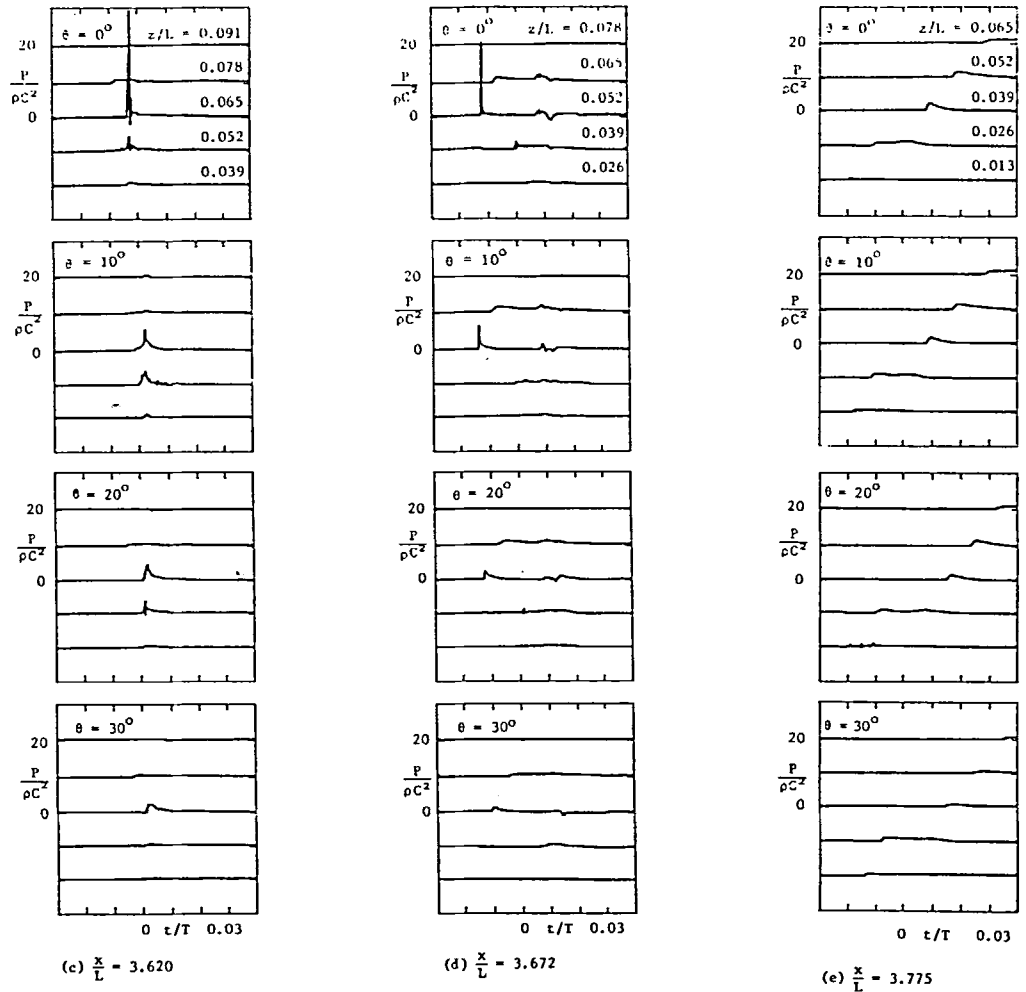


Fig. 3. Distributions of pressure time histories at various cylinder locations ($D/L = 0.88$)

Fig. 3 cont'd



3. RESULTS

3.1 Pressure distributions and characteristics

Selected pressure time histories obtained from the present study are shown in Figs. 3a-e, 4 and 5a, b. Each set of pressure records (e.g., Fig. 3c, $\theta = 0^\circ$) is obtained simultaneously from a single run of the experiments. Note, however, that pressures within the impact region varied significantly between repeated experiments (see Section 3.3). Despite the variability, these pressures do exhibit repeatable characteristics.

Figures 3a-e show the impact pressures obtained with a cylinder of diameter $D/L = 0.088$, at locations in the range $x/L = 3.645-3.775$ (N.B. Cylinder locations are defined by the edge of cylinder nearest to the incident wave front). It can be seen from these pressure records that, at cylinder locations $x/L = 3.568, 3.620$ and 3.672 , the pressures are characterised by an impact region where the pressure maxima are high ($> 10\rho C^2$, where ρ is the water density and C is the phase speed), and the pressure rise times are short ($< 0.002 T$). These pressures, subsequently referred to as the impact pressures, are also characterised by oscillations immediately following the pressure maxima. A version of Fig. 3c, $\theta = 0^\circ$, with the time scale expanded, is presented in Fig. 4. From this figure, it is evident that the oscillations are simultaneous at elevations

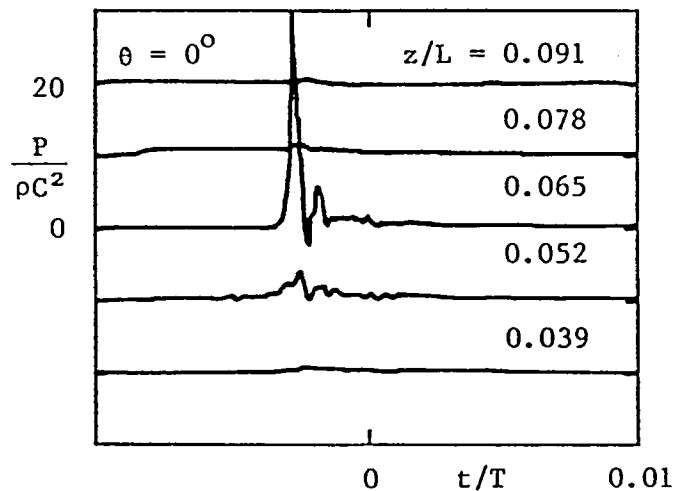


Fig. 4. Pressure time history at $x/L = 3.620$ ($D/L = 0.088, \theta = 0^\circ$)

$z/L = 0.065$ and 0.052 , but do not show up at other elevations.

The pressures away from the impact region are typically much lower than those within the impact region. The pressure maxima are less than $2\rho C^2$ and

the pressure rise times are more than 0.003 T. At each cylinder location and elevation, the pressure decreases as θ increases, but the pressure characteristics remain essentially the same (see Figs. 3a-e). However, the oscillatory characteristics associated with the impact region also diminish with the increase in θ . This suggests that the region of impulsive pressures is relatively small ($\Delta z/L \approx 0.03$; $\Delta\theta \approx 20^\circ$). During the experiments it was noted that these impact regions are also associated with air entrapment during impact. Air dynamics may therefore be a possible factor causing the pressure oscillations, and this will be consistent with the results from studies on wave impact on a vertical wall (Chan and Melville^{3,4}).

By comparing the pressure distributions obtained at different cylinder locations (Figs. 3a-e), it is evident that the pressure characteristics depend on the development of wave breaking prior to impact. At the upstream location, $x/L = 3.517$, the pressure time histories are smoothly varying and the pressure levels are low compared to those obtained downstream. The starting times of pressures (i.e. the time at which the pressures depart from zero) are delayed at higher elevations, consistent with the motion of the wave front past the cylinder.

Impulsive pressures are obtained at cylinder locations $x/L = 3.568$, 3.620 and 3.672 (Figs. 3b, c and d); at elevations $z/L = 0.065$ and 0.052. These elevations are just below $z/L = 0.067$, the maximum crest elevation observed in the absence of the cylinder. By considering the pressure characteristics of the impact region, it can be seen that the elevation of impact decreases from $z/L = 0.065$ to $z/L = 0.052$ as the cylinder location shifts downstream from $x/L = 3.568$ to $x/L = 3.672$. Further downstream, at $x/L = 3.775$, no impact pressures are evident and the pressure characteristics are similar to those observed at the upstream location $x/L = 3.517$.

A characteristic of pressures at $x/L = 3.568$ and 3.620 is the simultaneous occurrence of pressure maxima at elevations below the impact region. This is evident in Figs. 3b and 3c, at elevations below $z/L = 0.065$. Note that the simultaneous occurrence of pressure maxima will also imply a higher impact force compared to those obtained at other locations. A peculiar feature at these cylinder locations (i.e. at $x/L = 3.568$, 3.620 and 3.672) is the arrival time of pressures at the impact elevations. With the cylinder located at $x/L = 3.568$, the pressure arrival time at elevation $z/L = 0.078$ is just after the arrival of the impulsive pressure at $z/L = 0.065$. At the next downstream location ($x/L = 3.620$; Fig. 3c), the arrival time at $z/L = 0.078$ is earlier than that at the next lower elevation, $z/L = 0.065$, but comparable to that at $z/L = 0.052$. Yet further downstream ($x/L = 3.672$; Fig. 3d), the pressure arrival time at $z/L = 0.052$ is earlier than that at both the neighbouring elevations (i.e. at $z/L = 0.065$ and 0.039). Also, at the latter cylinder location, $x/L = 3.672$, the pressure signals exhibit double peaks in the time histories, with the second peak being non-impulsive. It should be noted that the above pressure characteristics obtained at the three cylinder locations (Figs. 3b-d), particularly the pressure arrival times, are typical of the results obtained from repeated experiments. As discussed later in Section 4, these characteristics may be attributed to the development of wave plunging prior to impact on the cylinder.

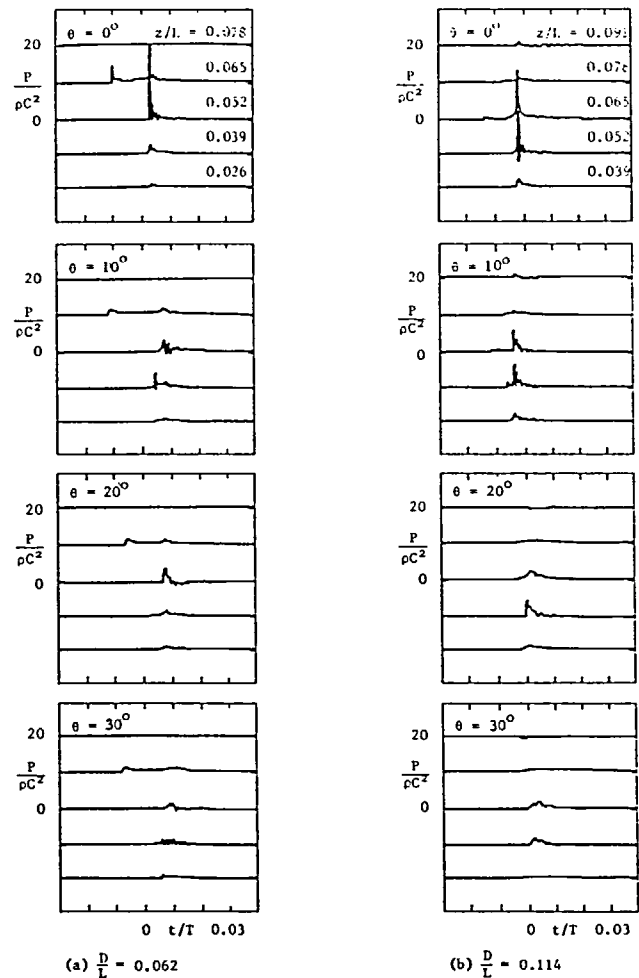


Fig. 5. Distributions of pressure time histories at $x/L = 3.620$

3.2 Variation of pressure characteristics with cylinder size

For the present study, experiments were also conducted with cylinder diameters $D/L = 0.062$ and 0.114, but with the same incident wave conditions far upstream. Detailed results are presented in Zhou²¹. Due to the similarity in the results obtained for different cylinder size, only selected distributions are presented in this paper for comparison.

Figures 5a and b show the typical pressure distributions obtained at $x/L = 3.620$ with cylinders of diameter $D/L = 0.062$ and 0.114 respectively. These figures are compared with Fig. 3c, the corresponding distribution for $D/L = 0.088$. From these figures, it is evident that similar pressure distributions and characteristics are obtained for the three cylinders. Impulsive pressures, characterised by the high pressure maxima and the oscillations, are evident in all three cases at elevations $z/L = 0.065$ and 0.052. These oscillations diminish with increasing θ , accompanied by a decrease in the pressure maxima at all the corresponding elevations. The earlier arrival time of pressures at the elevation just above that exhibiting impulsive pressures is also evident in all three cases for this particular cylinder location.

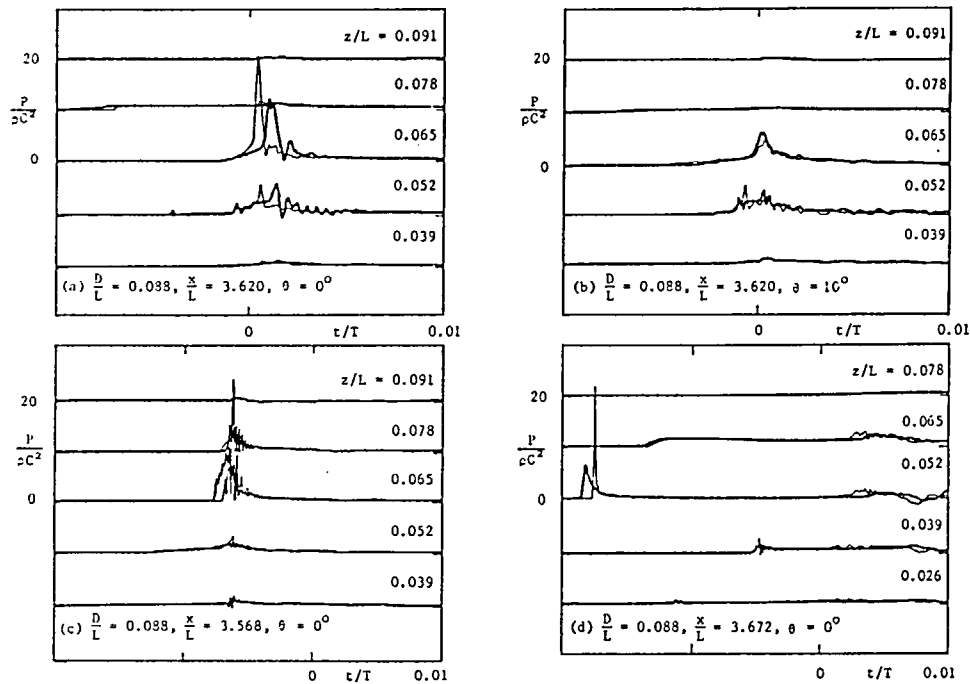


Fig. 6. Comparison of pressure time histories from repeated experiments

3.3 Variability in pressure time histories

As mentioned earlier in Section 3.1, the impulsive pressures vary significantly when the experiments are repeated with essentially identical conditions. This may be anticipated since the impulsive pressures are associated with wave breaking which yields an irregular and turbulent wave front prior to impact on the cylinder. This section examines, in further detail, the differences between the pressure characteristic of repeated runs. Selected results corresponding to a cylinder diameter of $D/L = 0.088$ are presented in Figs. 6a-d to show the variability associated with different azimuthal angle (θ) and cylinder location (x/L).

Figure 6a depicts the typical variability of pressures obtained at $x/L = 3.620$ ($\theta = 0^\circ$). It is evident from this figure that the main differences between the two repeated runs are in the impulsive pressures at $z/L = 0.065$ and 0.052 . The difference in the pressure maxima at $z/L = 0.065$ is about $10\rho C^2$; comparable to the pressure maximum obtained in one of the runs. Much higher differences ($> 20\rho C^2$) have been obtained in the present study. Also noted in this comparison is the difference in the frequency of pressure oscillations between the two runs, suggesting a difference in the air dynamics if the latter does contribute to the pressure oscillations.

Despite the significant variability in the impulsive pressures, the pressures at elevations away from the impact region are repeatable. This is evident at elevations $z/L = 0.039, 0.078$ and 0.091 (Fig. 6a) and in the pressure distributions obtained for $\theta = 10^\circ$ (Fig. 6b). Within the impact regions, pressures are also repeatable approximately $0.005 T$ after the occurrence of pressure maxima. These results suggest that significant variabilities are present only locally in time and space

and are associated only with the impulsive pressures within the impact region.

Similar variabilities are also obtained at other cylinder locations and for other cylinder diameters. The variabilities obtained at $x/L = 3.568$ and 3.672 are shown respectively in Figs. 6c and d. It should, however, be noted that pressures at cylinder locations further upstream are very repeatable.

3.4 Ensemble averaged time histories

The above results have illustrated the high variability of impact pressures, particularly in the pressure maxima and the pressure oscillations. Ensemble averages are therefore obtained to yield the mean pressure characteristics. Given the fact that pressure variabilities are associated with the impulsive pressures, an ensemble average of results obtained from repeated experiments will filter out the high pressure maxima and the pressure oscillations. Consequently, the ensemble average should be a good indication of the hydrodynamics of impact, since the impulsive and oscillatory character of the pressures may in turn be attributed to the trapped air dynamics.

Ensemble-averaged time histories of pressure obtained with a cylinder of diameter $D/L = 0.088$ are presented in Figs. 7a-c. Selected results for cylinder diameters $D/L = 0.062$ and 0.114 , at cylinder location $x/L = 3.568$, are presented in Figs. 8a and b respectively. Note that in evaluating the ensemble averages, the pressure time histories obtained from repeated experiments were synchronised at each elevation by the pressure arrival time. The pressure arrival time is defined as the time when the pressure first exceeds $0.05\rho C^2$. The average pressure arrival time at each cor-

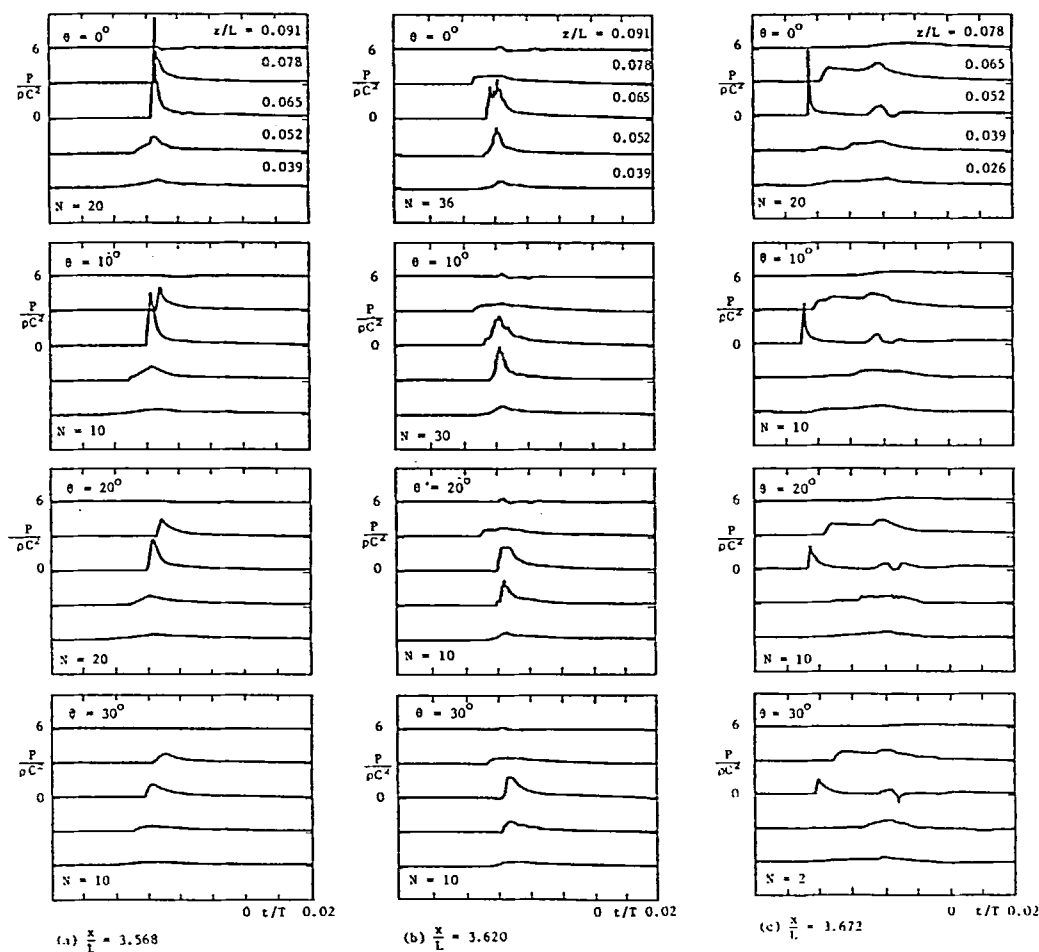


Fig. 7. Ensemble average of pressure time histories ($D/L = 0.088$; N is the number of repeated experiments)

responding elevation is used in the presentation of ensemble averaged time histories.

As shown in Figures 7a-c, the overall distribution of the mean pressure characteristics are similar to the typical results obtained from single runs of the experiments (see Figs. 3b-d, respectively). In particular, the distribution of high impulsive pressures remain approximately the same and the pressure maxima decreases with distance away from the impact region, both azimuthally and vertically. Mean pressures away from the impact region agree well with the pressures obtained from a single experiment and the relative pressure arrival times at elevations $z/L = 0.078$, 0.065 and 0.052 are retained in the ensemble averaged time histories. These results indicate the repeatability of the experiments. However, the maxima of pressures within the impact region range from $3\rho C^2$ to $9\rho C^2$, lower than the respective pressure maxima obtained from individual experiments. The difference is particularly significant at $x/L = 3.620$, $z/L = 0.065$ (see Figs. 3c and 7b); but this is expected since the time at which the pressure maximum occurs fluctuates from one run of the experiment to another, and therefore the impulsive pressures will be subjected to smoothing by the averaging process.

The above result is also reflected in Figs. 9a-d, where standard deviations are plotted together with the ensemble-averaged time histories. Note that high stan-

dard deviations, comparable to the mean pressure levels, are evident at elevations where impulsive pressures are obtained. Also, the standard deviations decrease with the azimuth (θ) and with time after the duration of impact (Figs. 9a and b), suggesting that high standard deviations are associated with the impulsive pressures at the impact region. This result has been deduced in Section 3.3 based on the direct comparison of pressure time histories.

Similar observations can be made from the ensemble averages and standard deviations corresponding to the other two cylinders, diameters $D/L = 0.062$ and 0.114 (see Figs. 8a, b). Comparing the results in Figs. 7a, 8a and 8b, it appears that there is no significant influence of cylinder size on the pressure characteristics. However, the closer pressure arrival times at $z/L = 0.065$ and 0.078 , and the correspondingly higher pressure maxima do indicate that the impact load on the cylinder of diameter $D/L = 0.088$ is more impulsive. It should be noted that the number of runs used in obtaining the ensemble averages is not the same between cylinder sizes, and in the above comparison we have examined the characteristics of distributions for all values of θ .

3.5 Distribution of mean pressure maxima

Based on the ensemble-averaged pressure time histories, distributions of pressure maxima are obtained

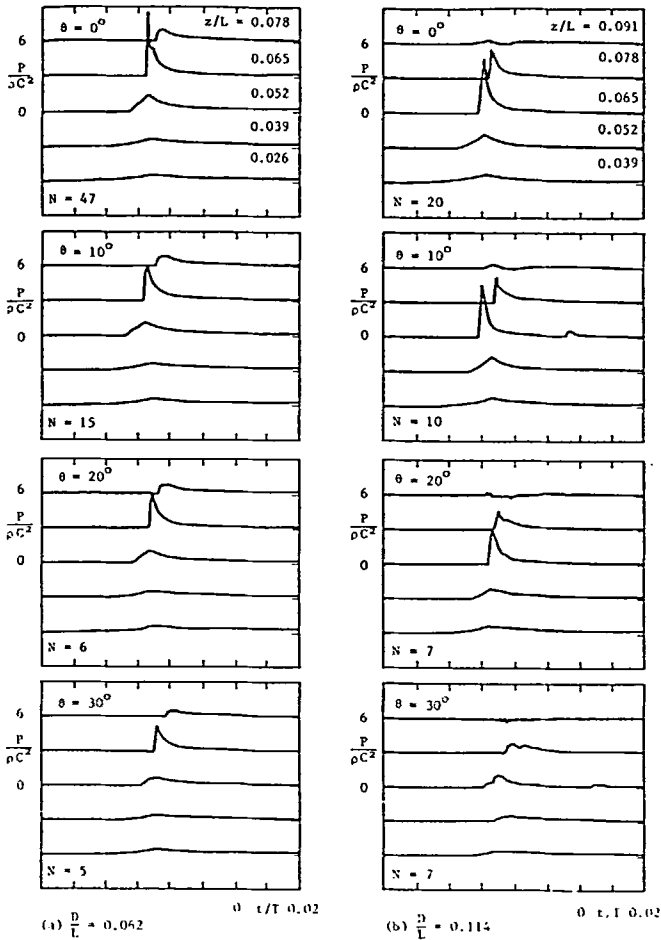


Fig. 8 Ensemble averages of pressure time histories ($x/L = 3.568$; N is the number of repeated experiments)

and presented in this section for further evaluation. Figs. 10a-c show the distributions corresponding to the three cylinders ($D/L = 0.062, 0.088$ and 0.114), at locations ranging from $x/L = 3.465$ to $x/L = 3.775$. These results are further compared with the mean peak pressures presented respectively in Figs. 11a-c. The mean peak pressure is the mean of peak pressures at corresponding elevations obtained from the time histories of repeated experiments. This is different from the maxima of ensemble averages, where the time histories are aligned and averaged before evaluating the maxima. Note that the distributions presented in Figs. 10 and 11 are limited by the vertical resolution of the data. A more rapid variation of the pressure maxima is expected near the elevations of impact.

It is noted from Figures 10a-c that the maxima of ensemble averages are highest when the cylinders are located at $x/L = 3.568$. The general decrease of pressure maxima with θ is also evident in these figures. The highest mean pressure maxima is about $9\rho C^2$, approximately ten times higher than the pressure maximum obtained upstream at $x/L = 3.465$. Of the three cylinders, that with $D/L = 0.088$ yielded the highest pressure maximum. This result is also evident in the distribution of mean peak pressures (Figs. 11a-c). However, the cylinder location yielding the highest peak pressure is at $x/L = 3.620$ rather than at $x/L = 3.568$. At locations $x/L = 3.568, 3.620$ and 3.672 , the mean peak pressures are higher than the corresponding pressure maxima obtained from the ensemble-averaged time histories. Further upstream, at $x/L = 3.465$ and 3.517 , the mean peak pressures are comparable to the maxima of the ensemble-averaged time histories. The mean peak pressures corresponding to the cylinder of diameter $D/L = 0.088$ are still higher than those obtained with the other two cylinders. The highest mean peak pressure is

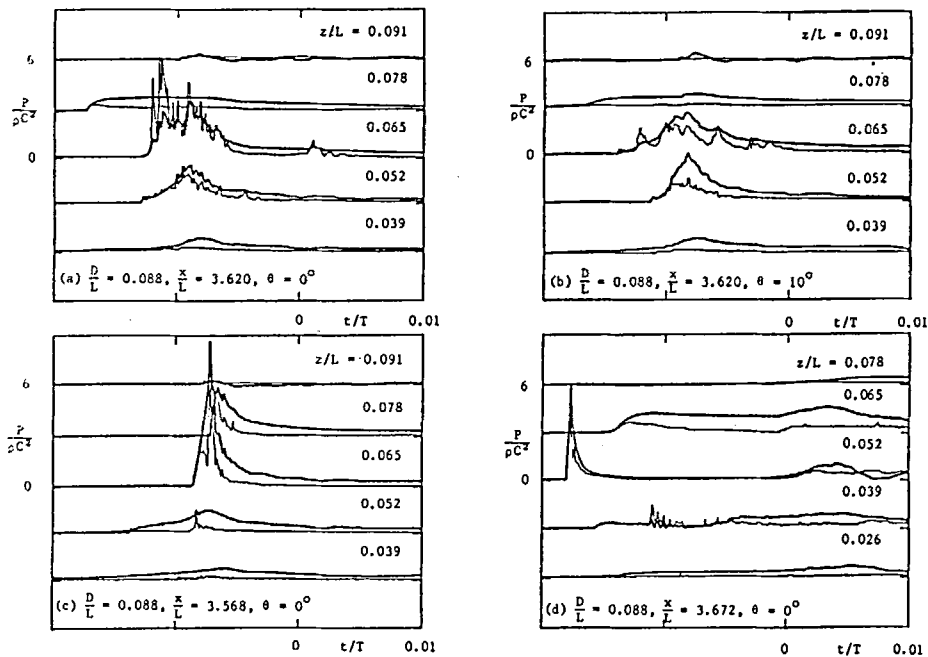


Fig. 9. Ensemble averages (—) and standard deviations (---) of pressure time histories

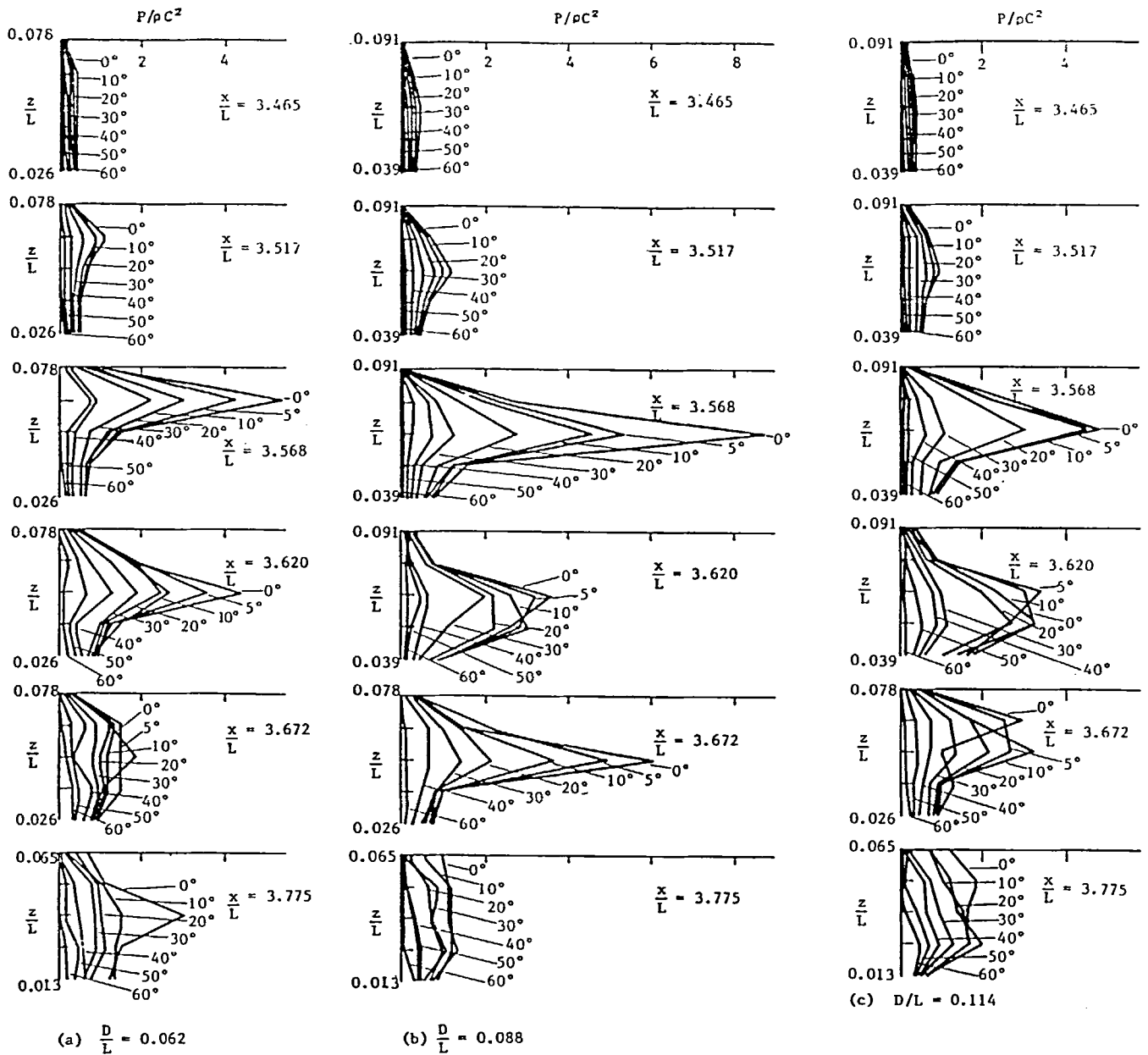


Fig. 10. Vertical distributions of pressure maxima obtained from ensemble average

about $16\rho C^2$ (Fig. 11b), approximately twenty times higher than the peak pressure obtained upstream at $x/L = 3.465$. The highest peak pressure obtained in this series of experiments is about $32\rho C^2$.

The azimuthal distributions of the pressure maxima discussed above have also been evaluated. Detailed plots of the distributions can be found in Zhou²¹. From the distributions, it is noted that the pressure maxima decrease significantly from $\theta = 0^\circ$ to $\theta = 60^\circ$. Except for a few cases at the elevation of impact, the pressure maxima approximately follow a cosine square decay with θ . At the elevations where pressures are more impulsive, the pressure maxima decrease exponentially with θ .

In view of the above observations, the distributions of pressure maxima have been fitted with cosine square distributions and where appropriate by the exponential

distribution. Further modification is, however, needed for the cosine square distribution, and may be approximately derived as follows. With reference to the control volume indicated in Fig. 12, the fluid with incident velocity v changes its momentum when it reaches the cylinder boundary. Conservation of momentum in the radial direction then leads to

$$F + F^* = d(mv)/dt = \rho v^2 dy dz \cos \theta \quad (1)$$

where F is the reaction force from the cylinder boundary on the control volume, and F^* is the radial component of fluid boundary force on the control volume. Dividing the above equation by the elemental area, $dsdz$, yields the equation

$$p + p^* = \rho v^2 \cos^2 \theta \quad (2)$$

Table 2: Azimuthal distributions of peak pressures

$$p/p_0 = \cos^2\theta (1 - M \sin\theta) \quad \text{or} \quad p/p_0 = \exp(-k\theta); \quad 0^\circ < \theta < 90^\circ$$

(a) Coefficients (M or k) corresponding to pressure maxima obtained from ensemble-averaged time histories.

z/L	$x/L = 3.465$	3.517	3.568	3.620	3.672	3.775
	(D/L = 0.062)					
0.078	M = 0.98	M = 0.74	M = 0.75	M = 0.60	M = 0.53	
0.065	M = 0.63	M = 0.51	M = 0.96	M = 0.32	M = 0.31	k = 0.074
0.052	M = 0.38	M = 0.50	M = 0.76	M = 0.79	k = 0.033	M = 0.54
0.039	M = 0.20	M = 0.25	M = 0.36	M = 0.26	M = -0.19	k = 0.059
0.026	M = -0.29	M = -0.33	M = -0.24	M = -0.28	M = -0.43	M = 0.38
0.013						M = 0.45
	(D/L = 0.088)					
0.091	M = 0.58	k = 0.046	k = 0.034	M = 0.08		
0.078	M = 0.74	M = 0.72	M = 0.99	M = 0.34	M = 0.45	
0.065	M = 0.64	M = 0.81	k = 0.074	M = 0.82	M = 0.54	k = 0.055
0.052	M = 0.43	M = 0.55	M = 1.00	M = 0.90	k = 0.057	M = 0.75
0.039	M = 0.17	M = 0.26	M = 0.68	M = 0.70	M = 0.04	M = 0.57
0.026					M = 0.37	M = 0.36
0.013						M = -0.26
	(D/L = 0.114)					
0.091	k = 0.044	k = 0.057	M = 0.91	M = 0.65		
0.078	M = 0.71	M = 0.66	M = 0.99	M = 0.59	M = 0.53	
0.065	M = 0.67	M = 0.84	k = 0.074	M = 0.99	M = 0.85	k = 0.058
0.052	M = 0.40	M = 0.59	M = 0.94	M = 0.77	M = 0.31	M = 0.87
0.039	M = 0.09	M = 0.28	M = 0.55	M = 0.92	M = 0.42	M = 0.47
0.026					M = 0.11	M = -0.05
0.013						M = -0.36

(b) Coefficients (M or k) corresponding to mean peak pressures obtained from pressure time histories.

z/L	$x/L = 3.465$	3.517	3.568	3.620	3.672	3.775
	(D/L = 0.062)					
0.078	M = 0.74	M = 0.68	M = 0.97	M = 0.79	M = 0.59	
0.065	M = 0.53	M = 0.74	k = 0.066	k = 0.046	M = 0.67	M = 0.94
0.052	M = 0.40	M = 0.46	M = 0.83	k = 0.057	k = 0.044	M = 0.88
0.039	M = 0.18	M = 0.21	M = 0.39	M = 0.70	M = 0.18	M = 0.78
0.026	M = -0.39	M = -0.34	M = -0.21	M = -0.13	M = -0.50	M = 0.21
0.013						M = 0.09
	(D/L = 0.088)					
0.091	M = 0.83	M = 0.88	k = 0.058	M = 0.93		
0.078	M = 0.57	M = 0.68	k = 0.055	k = 0.056	M = 0.35	
0.065	M = 0.61	M = 0.80	k = 0.076	k = 0.069	M = 0.84	M = 0.94
0.052	M = 0.41	M = 0.57	k = 0.056	M = 0.78	k = 0.064	M = 0.88
0.039	M = 0.17	M = 0.25	k = 0.038	M = 0.14	M = 0.48	M = 0.78
0.026					M = 0.21	M = 0.21
0.013						M = 0.09
	(D/L = 0.114)					
0.091	M = 0.64	M = 0.96	M = 0.87	k = 0.034		
0.078	M = 0.62	M = 0.61	M = 1.00	M = 0.81	M = 0.65	
0.065	M = 0.70	M = 0.86	k = 0.075	k = 0.067	k = 0.05	M = 0.67
0.052	M = 0.37	M = 0.59	M = 0.99	k = 0.058	M = 0.87	M = 0.84
0.039	M = 0.04	M = 0.27	M = 0.51	k = 0.045	M = 0.67	M = 0.81
0.026					M = 0.18	M = 0.23
0.013						M = -0.07

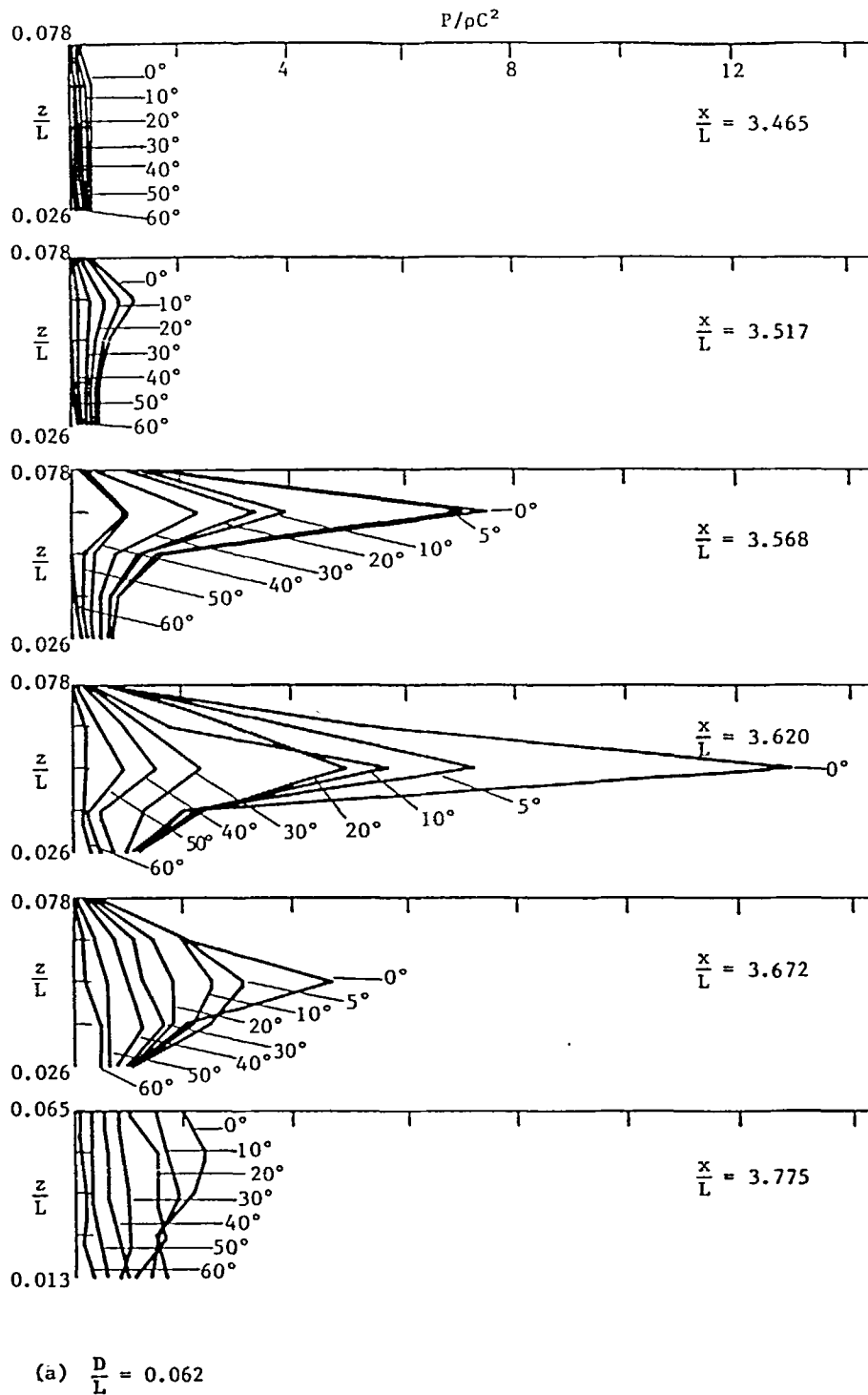


Fig. 11. Vertical distributions of mean peak pressures

where p and p^* are the pressures corresponding to F and F^* .

The above equation may be rewritten as

$$p = \rho v^2 \cos^2 \theta (1 - K) \quad (3)$$

where K is a non-dimensional coefficient dependent on θ . Based on least square fit, it is found that for practical purposes K may be expressed as a function of $\sin \theta$ and the above equation may be expressed as

$$p = p_0 \cos^2 \theta (1 - M \sin \theta) \quad (4)$$

where p_0 is the peak pressure at $\theta = 0^\circ$ and M is a constant. At elevations with high impulsive pressures, the exponential distribution is given by

$$p = p_0 \exp(-k\theta) \quad (5)$$

The above equations appear to fit the data remarkably well, and the results are presented in Table 2. For the

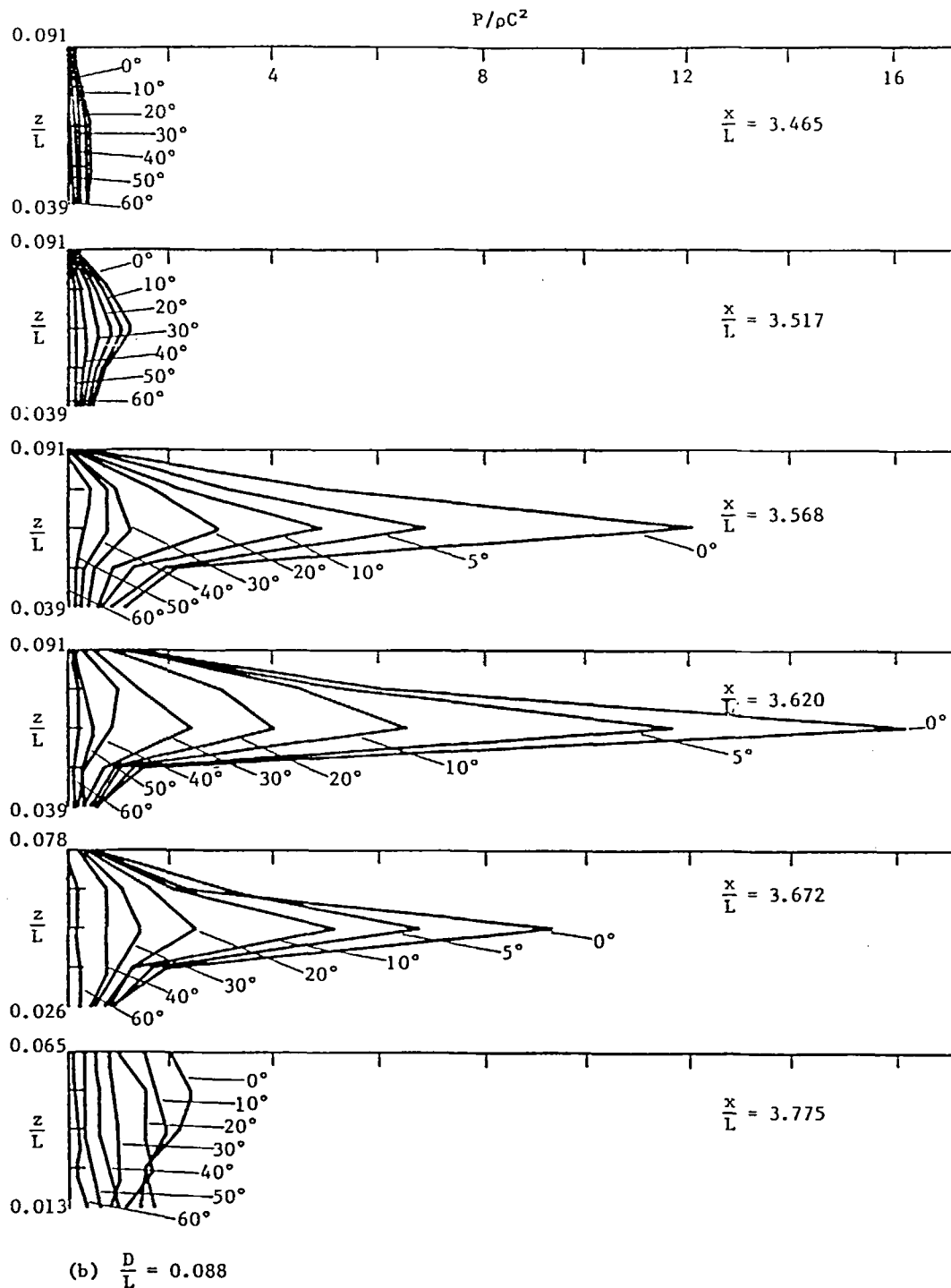


Fig. 11. cont'd

distributions of pressure maxima obtained from ensemble averages, M ranges from -0.4 to 1.0 and k ranges from 0.03 to 0.07 . For the mean peak pressures, M ranges from -0.5 to 1.0 and k ranges from 0.04 to 0.08 . We emphasize that the above equations are purely empirical and are intended to provide a simple correlation of the pressure maxima with the azimuth, and be useful in the preliminary analysis of wave impact loads on cylinders. At elevations near the impact elevation, both the cosine square fit and the exponential fit may be

used, and in the results presented in Table 2 we chose the best fit.

4. DISCUSSION AND CONCLUSION

In this paper, detailed pressure measurements have been obtained and presented to yield a better understanding of plunging wave impact on cylinders. The results show that wave impact leads to impulsive pressures which are

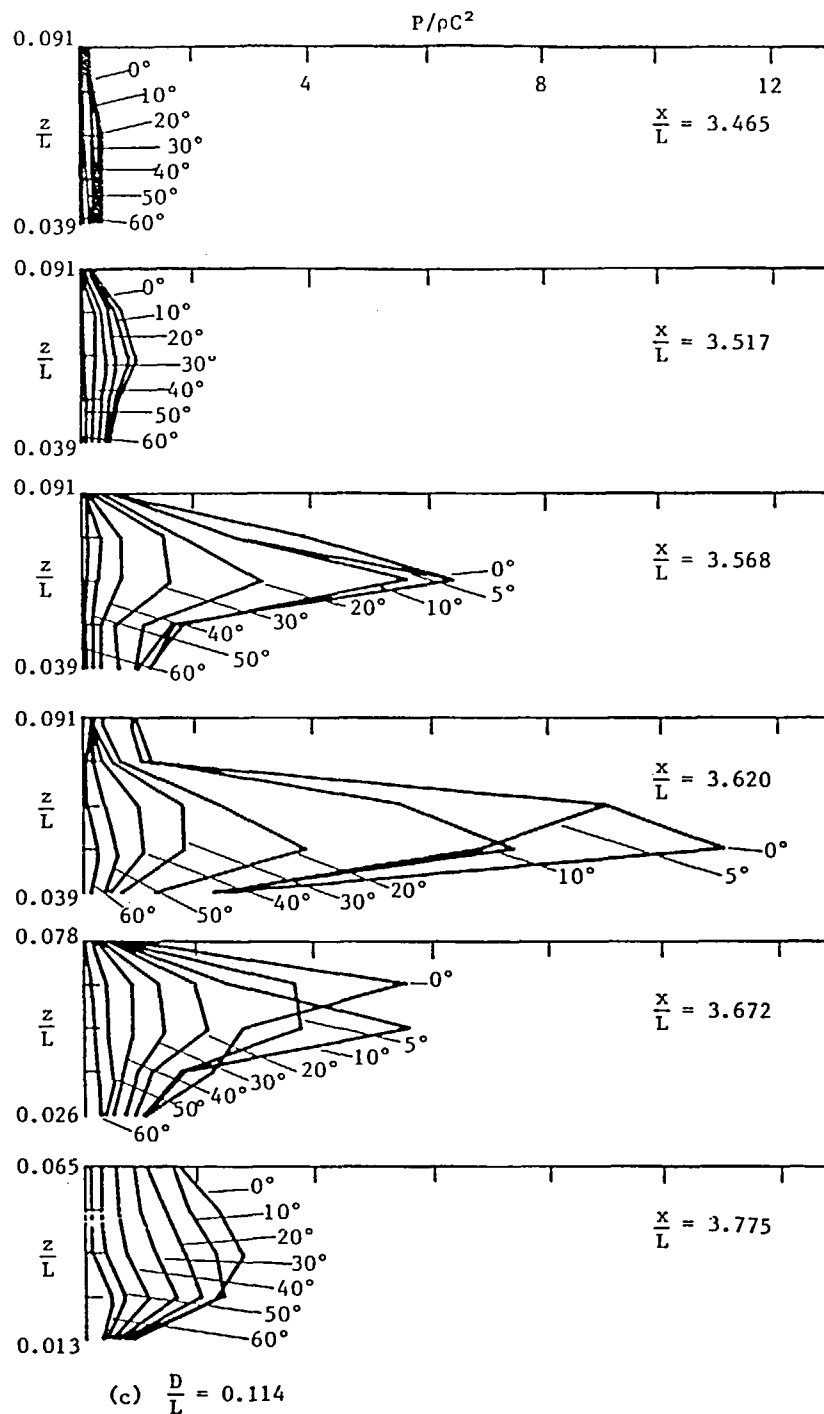


Fig. 11. cont'd

locally distributed in both space and time ($\Delta z \approx 0.03 L$, $\Delta \theta \approx 20^\circ$; $\Delta t \approx 0.01T$), and are characterised by high pressure maxima ($3-30\rho C^2$) followed by pressure oscillations. These characteristics, which may be associated with air entrapment during impact, fluctuate significantly even for essentially identical incident wave conditions. Both the pressure maxima and the pressure oscillations diminish with distance away from the impact region, and with time after the onset of impact.

Pressure characteristics associated with changes in the cylinder location have also been obtained. The results show that impact pressures can be obtained over a range

of cylinder locations ($\Delta x/L > 0.1$) rather than one critical location. Also, the pressure characteristics depended significantly on the cylinder location relative to the wave breaking location. These pressure characteristics (e.g., Fig. 3a-e) are nevertheless consistent with the development of wave plunging prior to impact, and may be explained with reference to Figs 13a-e. With the cylinder located far upstream (Fig. 13a), the wave will propagate past the cylinder without any impact, and the pressures will be non-impulsive (Fig. 3a). If the cylinder location is shifted downstream, wave breaking will eventually develop prior to impact (Fig.

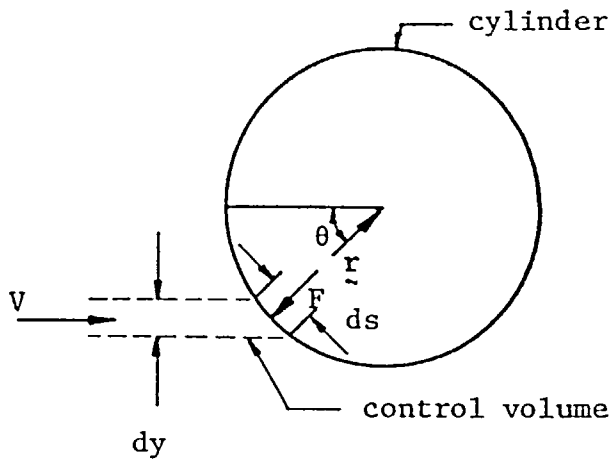


Fig. 12. Definition sketch

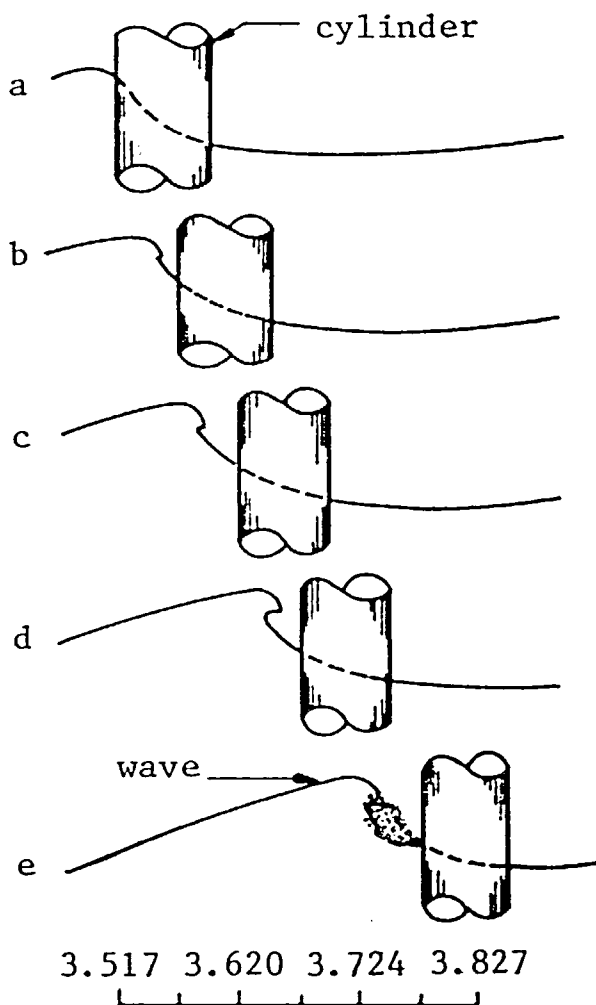


Fig. 13. Schematic of breaking wave impact on cylinder

13b) and impulsive pressures can be obtained at the elevation $z/L = 0.065$ (Fig. 3b). Wave breaking can be more developed prior to impact, as is the case in Fig. 13c, and the pressure arrival time at the elevation $z/L = 0.078$ can be earlier than that at $z/L = 0.065$ (Fig. 3c). Further downstream, wave plunging can develop to

the stage shown in Fig. 13d, where the development of a jet ahead of the wave front can lead to double peaks in the pressure signals (Fig. 3d). Yet further downstream (Fig. 13e), the wave can plunge back into the fluid ahead of the cylinder and the pressures will again be non-impulsive (Fig. 3e).

Given the variability of impact pressures, ensemble-averaged time histories and standard deviations have been obtained from repeated experiments and presented in this paper. The results show that high variability, or high standard deviations, are only associated with the impulsive pressures. This indicates the relative randomness in the impulsive pressures and the pressure oscillations, and is consistent with the fact that air entrapment on the breaking wave front is a highly variable phenomenon. Air dynamics may therefore be the main cause of pressure oscillations and the high pressure maxima. In fact, careful comparison of the ensemble-averaged time histories and the monitored pressure records (e.g. Figs. 7b and 3c) suggest that impact pressures consist of a basic hydrodynamic contribution, represented by the ensemble average, coupled with a perturbation contributed by the air dynamics. The relative randomness of the impulsive load further suggests that in a stochastic analysis of wave impact pressures, such as the procedures of Ochi and Tsai¹⁶, variability in the impact pressures should also be included. Note that the variability of impulsive pressures are not evident in the work by Ochi and Tsai¹⁶, who obtained peak pressures of about $1.4\rho C^2$.

Based on the ensemble averages, distributions of pressure maxima at various cylinder locations relative to the wave breaking location have also been obtained and presented. The pressure maxima range from about $1\rho C^2$ to $9\rho C^2$, depending on the cylinder location and the cylinder diameter. These distributions are further compared with the distributions of mean peak pressures which account for the contribution due to the air dynamics. The latter range from $1\rho C^2$ to $16\rho C^2$, higher than those from the ensemble averages. It should be noted that the ensemble-averaged characteristics, scaled by ρC^2 , may be used correspondingly in the prototype conditions. On the other hand, the mean peak pressures are dependent on the air dynamics which are still not well understood, and it is not clear how the results may be scaled to prototype conditions.

To illustrate the application of the above results, consider an offshore tension-leg platform subjected to breaking wave impact. If the diameter of the leg is 14 m and if the characteristic wave period is 10 s, then $D/L \approx 0.09$, and the results in this paper (Fig. 10) suggest that the mean pressure maxima will range from 240 kN/m^2 to 2190 kN/m^2 depending on the location of the cylinder relative to wave breaking location. Distributions of the mean pressure maxima may be obtained from Fig. 10. However, due to the neglect of possible contributions from the trapped air dynamics, the above results will be an underestimate of the mean peak pressures at locations yielding impulsive pressures. If the distributions of mean peak pressures from Fig. 11 are used, the predicted mean pressure maxima will range from 240 kN/m^2 to 3894 kN/m^2 ; but this is expected to be an overestimate since the trapped air at the wave front will be less compact under prototype conditions.

For practical purposes, such as the estimation of struc-

tural responses to wave impact, extrapolations of the present results to prototype conditions may also be achieved through the impulse – i.e. the integration of the pressure time histories over the duration of impact (about 0.01 T). It is noted from the present results that, despite the variability in the peak pressures, the impulse integrated over the duration of impact (about 0.01 T) are repeatable, and are also comparable to the impulse integrated from the ensemble averages. This impulse is sensibly independent of the air dynamics and may be used for extrapolating laboratory results to prototype scales. However, the procedure is possible only when the structural response time is much larger than the duration of impact. This is true for most practical situations. However, local areas of the structure may have response times comparable to or shorter than the integration time of an impulse, and in analysing the response of such local areas, the above procedure will not be applicable.

The characteristics of impact pressures presented in this paper are very similar to the results obtained by Chan and Melville⁴ for studies of wave impact on a vertical wall. In particular, the maximum of impulsive pressures presented in this paper, which range from $3\rho C^2$ to $32\rho C^2$, may be compared with a range of $3\rho C^2$ to $21\rho C^2$ obtained in the studies by Chan and Melville⁴ using identical incident wave conditions. The ensemble ranges are also comparable, but the highest mean pressure maxima obtained by Chan and Melville⁴ is $6.3\rho C^2$, slightly lower than the present result for impact on a cylinder (about $9\rho C^2$). Given the above agreement in pressure maxima, it is envisaged that impact pressures are not very sensitive to the horizontal variation of the structural geometry. This may be expected since breaking wave impact is a local phenomenon. On the other hand, the impact loads vary significantly with the relative structural location and possibly the trapped air dynamics. This suggests that in a stochastic analysis of the impact load, it is necessary to assess the probability of wave plunging at a particular location relative to the structure location and, for that location, the probability of exceeding a certain design load.

ACKNOWLEDGEMENTS

We wish to thank Mr Jack Crocker for his support in designing and building equipment for these experiments.

This research was supported by a grant from MIT/Sea Grant.

REFERENCES

- 1 Chan, E.S. and Melville, W.K. Deep water breaking wave forces on surface piercing structures, *Proc. OCEANS 84*, 1984, 565–570
- 2 Chan, E.S. and Melville, W.K. Deep water breaking wave forces on surface piercing structures, *Abstracts in depth, Intl. Conference on Theoretical & Applied Mechanics*, 1984, Lyngby, Denmark
- 3 Chan, E.S. and Melville, W.K. Plunging wave forces on surface piercing structures, *Proc. 6th Intl. Offshore Mechanics & Aortic Engrg. Symp.* II, 1987, 61–72
- 4 Chan, E.S. and Melville, W.K. Deep-water plunging wave pressures on a vertical plane wall, *Proc. R. Soc. Lond. A* 417, 1988, 95–131
- 5 Honda, T. and Mitsuyasu, H. Experimental study of breaking wave force on a vertical circular cylinder, *Coastal Engineering in Japan*, 1974, 17, 59–79
- 6 Dalton, C. and Nash, J.M. Wave slam on horizontal members of an offshore platform, *Proc. Offshore Technology Conf.*, Houston, Texas, May, paper No. OTC 2500, 1976, 769–779
- 7 Wiegel, R.L. Forces induced by breakers on pipes, *Coastal Engineering*, 1982, 1699–1715
- 8 Takagi, K., Naito, S. and Nakamura, S. The impact load and pressure acting on a vertical circular cylinder, *OMAE Conf.*, Japan, 1986, 242–249
- 9 Sawaragi, T. and Nochino, M. Impact forces of nearly breaking waves on a vertical circular cylinder, *Coastal Engineering in Japan*, 1984, 37, 249–263
- 10 Tanimoto, K., Takahashi, S., Kaneko, T. and Shiota, K. Impulsive breaking wave forces on an inclined pile exerted by random waves, *Coastal Engineering*, 1986, 2289–2302
- 11 Peregrine, D.H. Breaking waves on beaches, *An. Rev. Fluid Mech.*, 1983, 15, 149–178
- 12 Longuet-Higgins, M.S., F.R.S. and Cokelet, E.D. The deformation of steep surface waves on water, *Proc. R. Soc. Lond. A* 1976, 350, 1–26
- 13 Vinje, T. and Brevig, P. Numerical simulation of breaking waves, *Proc. 3rd Intl. Conf. on Finite Elements in Water Resources*, 1980, Univ. of Mississippi, Oxford, Mississippi
- 14 Vinje, T. and Brevig, P. 1981 Numerical calculation of forces from breaking waves, *Proc. Intl. Symp. Hydrodynamics*, 1981, Trondheim, Norway, 1–19
- 15 Morrison, J.R., Johnson, J.W. and O'Brien, M.P. Experimental studies of forces on piles, *Proc. 4th Conf. Coastal Engrg.*, 1953
- 16 Ochi, M.K. and Tsai, C.H. Prediction of impact pressure induced by breaking waves on vertical cylinders in random seas, *Applied Ocean Research*, 1984, 6(3)
- 17 Longuet-Higgins, M.S. Breaking waves in deep or shallow water, *Proc. 10th Symp. Nav. Hydrodynamics*, 1974, Office of Naval Res., 597–605
- 18 Greenhow, M., Vinje, T., Brevig, P. and Taylor, J. A theoretical and experimental study of the capsize of salter's duck in extreme waves, *J. Fluid Mech.*, 1982, 118, 221–239
- 19 Chan, E.S. Deepwater breaking wave forces on structures, *Sc.D. Thesis*, 1986, Dept. of Civil Engrg., MIT
- 20 Rapp, R. Laboratory measurements of deep water breaking waves, *Ph.D. Thesis*, 1986, Dept of Ocean Engrg., MIT
- 21 Zhou, D. S.M. Thesis, 1988, Dept of Civil Engrg., MIT